Finite-temperature Stress Calculations in Atomic Models using Moments of Position

Ranganathan Parthasarathy[1], Anil Misra[2], and Lizhi Ouyang[3]

[1]Postdoctoral Researcher, Department of Mathematical Sciences, Box 9616

Tennessee State University, 3500 John A Merritt Blvd, Nashville, TN 37209-1561, USA;

(corresponding author) Email: rparthas@tnstate.edu

[2]Professor, Department of Civil, Environmental and Architectural Engineering,

University of Kansas, 1530 W 15th St., Learned Hall, Lawrence, KS 66045-7609;

Email: amisra@ku.edu

[3]Professor, Department of Mathematical Sciences, Box 9616.

Tennessee State University, 3500 John A Merritt Blvd, Nashville, TN 37209-1561;

Email: louyang@tnstate.edu

Submitted for publication to:

Journal of Physics: Condensed Matter

Keywords: free energy, vibration tensor, vibration stress

ABSTRACT

Continuum modeling of finite temperature mechanical behavior of atomic systems requires refined description of atomic motions. In this paper, we identify additional kinematical quantities that are relevant for a more accurate continuum description as the system is subjected to step-wise loading. The presented formalism avoids the necessity for atomic trajectory mapping with deformation, provides the definitions of the kinematic variables and their conjugates in real space, and simplifies local work conjugacy. The total work done on an atom under deformation is decomposed into the work corresponding to changing its equilibrium position and work corresponding to changing its second moment about equilibrium position. Correspondingly, we define two kinematic variables: a deformation gradient tensor and a vibration tensor, and derive their stress conjugates, termed here as static and vibration stresses, respectively. The proposed approach is validated using MD simulation in NVT ensembles for fcc aluminum subjected to uniaxial extension. The observed evolution of second moments in the MD simulation with macroscopic deformation is inconsistent with the transformation of atomic trajectories through the deformation gradient using a generator function. Correspondingly, the vibration part of the Piola stress becomes particularly significant at high temperature and high tensile strain as the crystal approaches the softening limit. In contrast to the eigenvectors of the deformation gradient, the eigenvectors of the vibration tensor show strong spatial heterogeneity in the vicinity of softening. More importantly, the elliptic distribution of local atomic density transitions to a dumbbell shape, before significant non-affinity in equilibrium positions has occurred.

1. Introduction

In concurrent as well as hierarchical multiscale modeling, the computation of continuum scale quantities including internal energy, entropy, stress, strain and temperature from molecular dynamics (MD) simulations is ubiquitous. For example, in the recent past, MD has been used to study the microstructural origins of material failure in metallic glass, and the necessity for further investigation into "dynamic heterogeneities" has been strongly emphasized (1–4). In particular, the importance of an atomic level stress definition to study the local environment has been stressed (5). MD has also been used to study inter-atomic stress in simulation of ion-beam assisted deposition (2). The effects of cross-sectional shapes of silicon nanowires on their plasticity, stability and deformation, particularly with respect to dislocation nucleation, have also been investigated using MD simulation (6). The virial stress has been used in all these applications to calculate the atomic-level stress. Indeed, the virial stress expression is an invaluable computational diagnostic tool for evaluation of these continuum scale quantities for the study of several material science phenomena (7). The literature base in this line of research is rather vast and the above examples are for illustration only. In a solid mechanics discrete-to-continuum homogenization framework where the discrete scale is much larger than the atomic scale, for example in granular micromechanics (8–14), thermal vibration of particles is not relevant and the virial stress can be derived in a straightforward manner using the principles of virtual work (14,15). However, when the homogenization is from atomic to continuum scale at finite temperature, the effect of thermal vibration on the stress needs to be quantified. Finite temperature continuum stress from molecular simulation is most often computed using the virial stress expression. The expression for

virial pressure was originally proposed by Clausius and Maxwell, based upon the virial theorem of Clausius (16). In order to define the virial stress, the continuum space has been connected to the discrete scale in two ways: (i) coarse-graining or system-average approaches where each material point in the continuum space is composed of a sufficiently large number of atoms (9,14,16–28) and (ii) localization approaches where the continuum space is of atomic scale resolution and continuum definitions are obtained by smearing the influence of individual atoms across the space (7,29–36). In both (i) and (ii), the results can be averaged over a macroscopically small time interval. The virial stress itself has been derived using several approaches, including, term-by-term comparison of the balance laws in continuum and atomic scale (32,37–39), the statistical mechanics definition of stress (21,40), and computation of the free energy using quasi-harmonic approximation in reciprocal space (41), or a combination of these approaches. In particular, Kuzkin and Krivtsov (38,39,42–45) have derived Piola and Cauchy stress expressions from the atomistic scale using comparison of momentum balance between scales, and explicitly isolate the contributions to stress from (i) average atomic displacements and (ii) thermal vibration. In their seminal paper, Irving and Kirkwood (33) devised a somewhat distinct syncretic approach that utilizes a distribution function in phase space for obtaining expressions of the localized continuum quantities as well as their derivatives with respect to time. However, as pointed out by Zimmerman (7), this procedure is cumbersome since it requires the integration of a large number of functions including an infinite series of differential operators over phase space. Using a different approach, the virial stress has been derived from the Hamiltonian using the statistical mechanics definition of stress (see Eq. 4.3.22 in Weiner (41)). By definition, this method

involves ensemble averaging of the atomic scale quantities and has been widely used by a number of researchers (18,21,22,25,30,46). In these approaches, either atom-to-atom mapping is used between the undeformed and deformed atomic trajectories, or alternatively, quasi-harmonic approximation and the theory of small vibration is used to calculate the free energy and the corresponding stress conjugate (20,41). We note that approaches where the stress is calculated using comparison of momentum balance between discrete and continuous descriptions do not require atom-to-atom mapping between undeformed and deformed trajectories. On the other hand, in these approaches, work conjugacy of the obtained stress with rate of deformation or other strain measures does not follow spontaneously, as pointed out by Zhou (23). There are other important concerns regarding the equivalence of the virial stress and continuum mechanical stress at the boundaries of solids with atomic level inhomogeneity, particularly with respect to local stress on surface atoms, which are crucial in analyzing MD simulations of nanostructures from a continuum viewpoint (6,47). In this paper, however, we restrict our discussion to crystals which are homogeneous and periodic in the undeformed configuration.

While continuum stress measures have been formulated to account for non-affine deformations arising from atomic scale structural disorder (48,49), comparatively little attention has been devoted to an investigation of non-affinity due to thermal vibration (50–52) and its bearing on the calculation of continuum stress and strain from atomistic systems. Such investigation could be beneficial towards continuum interpretation of thermally activated processes, which play a crucial role in important phenomena including the onset of yield in crystalline metals (53), rejuvenation of metallic glasses by

thermal cycling (54), variation of creep mechanism in metals (55–57) and high entropy alloys (58) with temperature, elastic properties of crosslinked polymers (59,60) glass transition (61) and plastic deformation (62–65) of polymers under temperature and moisture gradients.

In this paper, we have reconsidered the stress calculation for atomic systems in quasi-static MD simulations. In particular, we (i) decompose the deformation kinematics of each atom based on change in equilibrium position and change in second moments about equilibrium positions, (ii) derive the stress measures conjugate to each of these kinematic deformation measures, and (iii) present numerical results for MD simulation of uniaxial deformation of fcc Aluminum. In section 2 we derive the expressions defining relevant stress tensors for atomic systems in a virtual work framework that includes the atomic vibration as an additional kinematic variable. To this end we introduce an atomic vibration tensor. As a result, we find a vibration stress tensor conjugate to the vibration tensor in addition to the static stress conjugate to the deformation gradient. For certain simple atomic systems, the vibration tensor is shown to be a function of deformation gradient. Consequently, the average Piola stress for a crystalline supercell is derived as a conjugate to the overall deformation gradient in section 2.2. We present our simulation and computation procedures in section 3, and numerical results in section 4.

2. Kinematics and Stress Measures

2.1. Role of atomic trajectory mapping

Under ergodicity, the macroscopic Piola stress (41,66) of a system of atoms occupying volume, V_o, with distribution function in phase space, ρ, can be defined as follows,

$$P_{ij} = \frac{1}{V_0}\int_{\Gamma} \frac{\partial H\left(q,p,F_{ij}\right)}{\partial F_{ij}} \rho \mathrm{d}q\mathrm{d}p = \frac{1}{V_0}\left\langle \frac{\partial H\left(r_k^a(t)\right)}{\partial F_{ij}} \right\rangle \tag{1}$$

where $H(q,p,F_{ij})$ is the Hamiltonian of the system, q and p are the generalized coordinates and momenta, F_{ij} is the deformation gradient, $r_k^a(t)$ is the position of the a^{th} atom at time t. Throughout the paper, subscripts have been used to represent the x, y or z coordinate, superscripts for the atom number, and angular braces represent the time average. Rewriting the Hamiltonian as sum of potential and kinetic energies, Eq. (1) is written as:

$$P_{gh} = \frac{1}{V_0}\left\langle \frac{\partial H\left(r_k^a(t)\right)}{\partial F_{gh}} \right\rangle = \frac{1}{V_0}\left\langle \frac{\partial \phi^{\mathrm{int}}\left(r_k^a(t)\right)}{\partial F_{gh}} \right\rangle + \frac{1}{V_0}\left\langle \frac{\partial K\left(p_k^a(t)\right)}{\partial F_{gh}} \right\rangle \tag{2}$$

where $\phi^{\mathrm{int}}\left(r_k^a(t)\right)$ is the potential energy of the system, $K\left(p_k^a(t)\right)$ is the kinetic energy of the system, and $p_k^a(t)$ is the momentum of atom a. In such a description, we note that $\frac{\partial \phi^{\mathrm{int}}\left(r_k^a(t)\right)}{\partial F_{gh}}$ is evaluated as $\frac{\partial \phi^{\mathrm{int}}\left(r_k^a(t)\right)}{\partial r_k^a(t)} \frac{\partial r_k^a(t)}{\partial F_{gh}}$. The second term of the RHS in Eq. (2) also requires similar mapping for the momenta. Thus, the trajectory-to-trajectory mapping between the deformed and undeformed configurations is essential in order to calculate the stress P_{gh}. However, establishing unique trajectory-to-trajectory mapping is non-trivial as discussed in Appendix A, therefore we follow an alternative approach in this paper.

2.2. Average stress in a supercell

Considering a crystalline supercell made of N atoms of a solid material, with boundaries deformed according to a specified deformation gradient, we recognize that the work done on the system, -dW, represents the work done in changing the equilibrium positions of the atoms, as well as the work done in changing the second moment about equilibrium

positions. The total potential energy of the system $\phi^{total} = \phi^{\text{int}} + \phi^{ext}$ is the sum of the energy of interaction of the atoms of the system with themselves (ϕ^{int}) as well as with an external agency (ϕ^{ext}) that is responsible for deforming the system.

At a constant temperature *T*, the total virtual work done on a single atom, a, can be written as:

$$\delta W^a = \int_{\Gamma} f_i^{ext,a} \delta r_i^a \rho \mathrm{d}p\mathrm{d}q = \left\langle f_i^{ext,a} \delta r_i^a \right\rangle \tag{3}$$

Where $f_i^{ext,a} = -\dfrac{\partial \phi^{ext}}{\partial r_i^a}$ is the external force acting on the atom and δr_i^a is the infinitesimal perturbation to $r_i^a(t)$. In a step-wise deformation process, at any step, the total potential energy can be taken as harmonic for small perturbations about the equilibrium position leading to the following approximation:

$$f_i^{ext,a} + f_i^{\text{int},a} = -\sum_b k_{ij}^{total,ab} \left(r_j^b - \bar{r}_j^b \right) \tag{4}$$

where

$$k_{ij}^{total,ab} = -\left(\frac{\partial f_i^{a,\text{int}}}{\partial r_j^b} + \frac{\partial f_i^{a,ext}}{\partial r_j^b} \right)\Bigg|_{r_i^p = \bar{r}_i^p, r_j^q = \bar{r}_j^q} = \left(\frac{\partial^2 \phi^{\text{int}}}{\partial r_j^a \partial r_i^b} + \frac{\partial^2 \phi^{ext}}{\partial r_j^a \partial r_i^b} \right)\Bigg|_{r_i^a = \bar{r}_i^a, r_j^b = \bar{r}_j^b}$$

is the local stiffness or force constant when atoms a and b are at their equilibrium positions. On the other hand, the internal force on atom a, under a general state of strain, and at any general position in its trajectory, defined as $f_i^{\text{int},a} = -\dfrac{\partial \phi^{\text{int}}}{\partial r_i^a}$, is more accurately estimated as follows using a quasi-harmonic assumption. We remark that a similar approximation to the second order has been adopted (38,39) in approximating the force on the atom at its instantaneous position. However, in (39) and (38), the atomistic-to-

continuum bridging was performed using comparison of momentum balance, while we perform the same using equivalence of virtual work at the two scales.

$$f_i^{\text{int},a} = \bar{f}_i^{\text{int},a} - \sum_q k_{ij}^{\text{int},ab}\left(r_j^b - \bar{r}_j^b\right) - \sum_l \sum_q \frac{\partial k_{ij}^{\text{int},ab}}{\partial r_k^c}\left(r_j^b - \bar{r}_j^b\right)\left(r_k^c - \bar{r}_k^c\right)$$

where $\bar{f}_i^{\text{int},a} = -\left.\frac{\partial \phi^{\text{int}}}{\partial r_i^a}\right|_{r_i^a = \bar{r}_i^a}$ is the internal force on the atom at its equilibrium position and

$$k_{ij}^{\text{int},ab} = -\left(\left.\frac{\partial f_i^{a,\text{int}}}{\partial r_j^b}\right)\right|_{r_i^a=\bar{r}_i^a, r_j^b=\bar{r}_j^b} = \left(\left.\frac{\partial^2 \phi^{\text{int}}}{\partial r_j^a \partial r_i^b}\right)\right|_{r_i^a=\bar{r}_i^a, r_j^b=\bar{r}_j^b} \tag{5}$$

is the local stiffness or force constant with respect to the internal potential. Substituting for $f_i^{a,\text{int}}$ and using Eq. (4) in Eq. (3) we get,

$$\begin{aligned}\delta W^a = -\bar{f}_i^{\text{int},a}\delta\bar{r}_i^a - \sum_b \left(k_{ij}^{total,ab} - k_{ij}^{\text{int},ab}\right)\left(\left\langle \delta r_i^a r_j^b \right\rangle - \delta\bar{r}_i^a \bar{r}_j^b\right) \\ - \left\langle \sum_l \sum_q \frac{\partial k_{ij}^{\text{int},ab}}{\partial r_k^c}\left(r_j^b - \bar{r}_j^b\right)\left(r_k^c - \bar{r}_k^c\right)\delta r_i^p \right\rangle\end{aligned} \tag{6}$$

Now defining the second moment about equilibrium atomic positions for atoms *a* and *b* as $\beta_{ij}^{ab} = \left\langle r_i^a r_j^b \right\rangle - \bar{r}_i^a \bar{r}_j^b$, the first variation of β_{ij}^{ab} can be written as

$$\delta\beta_{ij}^{ab} = \left\langle \delta r_i^a r_j^b \right\rangle + \left\langle r_i^a \delta r_j^b \right\rangle - \delta\bar{r}_i^a \bar{r}_j^b - \bar{r}_i^a \delta\bar{r}_j^b .$$

From Eq. (6), the total work done on all the atoms can be written as follows (see Appendix B for details):

$$\delta W = \sum_{a=1}^{N} -\bar{f}_i^{\text{int},a}\delta\bar{r}_i^a + \frac{1}{2}\sum_{a=1}^{N}\sum_{b=1}^{N}\left(k_{ij}^{\text{int},ab} - k_{ij}^{total,ab}\right)\left(\delta\beta_{ij}^{ab}\right) + \frac{1}{2}\sum_{a=1}^{N}\sum_{b=1}^{N}\delta k_{ij}^{\text{int},ab}\beta_{jk}^{ab} \tag{7}$$

We assume $k_{kl}^{total,ab}$ and $k_{kl}^{\text{int},ab}$ to be equal; therefore the second term of Eq. (7) reduces to zero. Further, we rewrite:

$$\delta k_{ij}^{\text{int},ab} = \delta k_{ij}^{ab,0} + \left(\delta k_{ij}^{ab,T} - \delta k_{ij}^{ab,0}\right) \tag{8}$$

where $k_{ij}^{ab,0}$ are the force constants at zero temperature (see step 4 of section 3.1 for calculation procedure) and $k_{ij}^{ab,T}$ are the force constants at a finite temperature T (see section 3.3 for calculation procedure). We note that $\delta k_{ij}^{ab,0}$ represents the change in force constants caused solely by the change in atomic equilibrium positions, while $\delta k_{ij}^{ab,T}$ represents the total change in force constants due to the change in atomic equilibrium positions as well as the change in atomic trajectories. Therefore, Eq. (8) can be rewritten as:

$$\delta k_{ij}^{\text{int},ab} = \frac{\partial k_{ij}^{ab,0}}{\partial F_{kl}} \delta F_{kl} + \sum_{c=1}^{n} \frac{\partial}{\partial G_{kl}^{0c}} \left(k_{ij}^{ab,T} - k_{ij}^{ab,0} \right) \delta G_{kl}^{0c} \tag{9}$$

where we introduce G_{mn}^{ab} as the normalized second moment about equilibrium atomic position for atoms *a* and *b*, which we henceforth refer to as the vibration tensor. The normalization factor $K = \frac{\left(\frac{1}{2} m^a \omega_D^2 \right)}{k_B T}$ where m^a is the mass of atom *a*, ω_D is the Debye frequency of the material under study at 0% strain, k_B is the Boltzmann constant, and T is the temperature. $G_{kl}^{0c} = \frac{1}{N} \sum_{a=1}^{N} G_{kl}^{ac}$ is the average vibration tensor in the supercell representing interaction between an atom and its c^{th} neighbor, and n represents the neighbor number up to which the interaction is significant. F_{ij} is the deformation gradient in the supercell assumed to be uniform so that the change in atomic equilibrium positions is affine. We now substitute: (a) $\bar{r}_i^a = F_{ij} \bar{R}_j^a$, (b) $\delta G_{mn}^{ab} = K \left(\delta \beta_{mn}^{ab} \right)$, and (c) Eq. (9) in Eq. (7) to obtain:

$$\delta W = \left[\sum_{a=1}^{N} -\bar{f}_i^{\text{int},a} \bar{R}_j^a + \frac{1}{2} \sum_{a=1}^{N} \sum_{b=1}^{N} \frac{\partial k_{kl}^{ab,0}}{\partial F_{ij}} \beta_{kl}^{ab} \right] \delta F_{ij} + \sum_{c=1}^{n} \left[\frac{1}{2K} \sum_{a=1}^{N} \sum_{b=1}^{N} \frac{\partial \left(k_{kl}^{ab,T} - k_{kl}^{ab,0} \right)}{\partial G_{ij}^{0c}} \beta_{kl}^{ab} \right] \delta G_{ij}^{0c} \tag{10}$$

We note that Eq. (10) represents the change in free energy of the system at constant temperature. Under the condition of affine transformation inside a supercell whose primitive cell contains only one atom, we can assume a uniform F_{ij} and a uniform G_{kl}^{0c} inside the supercell, where G_{kl}^{0c} is defined between any atom (all atoms are equivalent) and its c[th] neighbor. Then, Eq. (10) can be decomposed into two parts: (a) the change in free energy due to change in equilibrium positions of atoms and (b) the change in free energy due to change in the second moments about equilibrium atomic positions. They can be represented as:

$$\mathrm{d}\Psi^F = \left(-\sum_{a=1}^{N} \bar{f}_i^{\text{int},a} \bar{R}_j^a + \frac{1}{2} \sum_{a=1}^{N} \sum_{b=1}^{N} \frac{\partial k_{kl}^{ab,0}}{\partial F_{ij}} \beta_{kl}^{ab} \right) \delta F_{ij} \tag{11}$$

$$\mathrm{d}\Psi^G = \sum_{c=1}^{n} \left[\frac{1}{2K} \sum_{a=1}^{N} \sum_{b=1}^{N} \frac{\partial \left(k_{kl}^{ab,T} - k_{kl}^{ab,0} \right)}{\partial G_{ij}^{0c}} \beta_{kl}^{ab} \right] \delta G_{ij}^{0c} \tag{12}$$

where n is the neighbor number beyond which the terms β_{ij}^{0n} are insignificant. From Eq. (12), the average static stress in the supercell is defined as:

$$T_{ij} = \frac{1}{V^0} \frac{\partial \Psi}{\partial F_{ij}} = \frac{1}{V^0} \left[-\sum_{a=1}^{N} \bar{f}_i^{\text{int},a} \bar{R}_j^a + \frac{1}{2} \sum_{a=1}^{N} \sum_{b=1}^{N} \beta_{kl}^{ab} \frac{\partial k_{kl}^{ab,0}}{\partial F_{ij}} \right] \tag{13}$$

and the average vibration stress in the supercell corresponding to the atom-neighbor pair between an atom and its c[th] neighbor is defined as:

$$Q_{ij}^{0c} = \frac{1}{V^0} \frac{\partial \Psi}{\partial G_{ij}^{0c}} = \frac{1}{V^0} \left(\frac{1}{2K} \sum_{a=1}^{N} \sum_{b=1}^{N} \beta_{kl}^{ab} \frac{\partial \left(k_{kl}^{ab,T} - k_{kl}^{ab,0} \right)}{\partial G_{ij}^{0c}} \right) \tag{14}$$

where V^0 is the underformed volume of the supercell. For crystals with only one atom in the primitive cell, within the elastic regime, a constitutive relationship of the form $G_{ij}^{0c} = f\left(F_{ij}, T\right)$ can be defined. Under this condition, it is possible to express $\delta G_{ij}^{0c} = \dfrac{\partial G_{ij}^{0c}}{\partial F_{kl}} \delta F_{kl}$. Therefore, both the static and vibration stresses from Eqs. (13) and (14) may be viewed as conjugate to F_{ij} and the average Piola stress in the supercell can be written as the following sum:

$$P_{ij} = P_{ij}^{T} + P_{ij}^{Q} \tag{15}$$

In Eq. (15), the static part of the average Piola stress is given as:

$$P_{ij}^{T} = \frac{1}{V^0}\left[-\sum_{a=1}^{N} \bar{f}_i^{\text{int},a} \bar{R}_j^a + \frac{1}{2}\sum_{a=1}^{N}\sum_{b=1}^{N} \beta_{kl}^{ab} \frac{\partial k_{kl}^{ab,0}}{\partial F_{ij}} \right] \tag{16}$$

while the vibration part of the average Piola stress is:

$$P_{ij}^{Q} = \frac{1}{V^0}\left(\frac{1}{2K}\sum_{a=1}^{N}\sum_{b=1}^{N} \beta_{kl}^{ab} \frac{\partial\left(k_{kl}^{ab,T} - k_{kl}^{ab,0}\right)}{\partial F_{ij}} \right) \tag{17}$$

In general, a relationship of the form $G_{ij}^{0c} = f\left(F_{ij}, T\right)$ is difficult to specify except for the case of homogeneous crystal with affine transformation. Comparing Eqs. (16) and (17) with the Mie-Gruneisen equation (67), the first term of Eq. (16) is similar to the "cold pressure", while the second term of Eq. (16), as well as the term in Eq. (17) are similar to the thermal pressure contribution, represented by the Gruneisen coefficient. We follow a similar approach as (38,39) in connecting the kinematics of the discrete system to continuum deformation, but compute the stress measures using equality of virtual work at continuum and atomic scales, rather than using momentum balance comparison between scales.

We note here that the second term of Eq. (16) bears resemblance to the kinetic contribution, typically arising from thermal vibrations, of the stress tensor defined by Hardy (32). It is noteworthy that in an ideal harmonic solid, the thermal stress does not contribute to work done. It is clear from Eq. (16) that the second term will vanish for such ideal cases. However in the classical formulations, such as that in Hardy, it is not clear under what conditions the kinetic contributions vanish. Consequently, the work conjugacy aspects of the kinetic contribution term in classical formulation needs careful reexamination (23).

3. Numerical Simulations

3.1. Molecular Dynamics simulation of fcc Aluminum under uniaxial tension

The derived formulation was evaluated using results from MD simulations. The simulation was performed using LAMMPS code (68) on a periodic supercell made of 10 X 10 X 10 primitive unit cells of face-centered cubic Aluminum using an embedded atom method (EAM) (69) potential. The triclinic non-orthogonal supercell contained 1000 atoms. Periodic boundary conditions (PBC) were used for the simulation in the three Cartesian directions to simulate an infinite crystal. The x, y and z axes were chosen to lie along the [100], [010] and [001] crystallographic directions. The simulation was performed in the following steps:

1. The supercell was first relaxed to zero stress state (P = 0) in the NPT ensemble using 0.5×10^6 time-steps with a time period of 1 fs. A Nose-Hoover thermostat was used to maintain the temperature at T = 300 K. The centroid of the supercell is maintained at a constant value for each time step. The dimensions of the supercell under zero-stress conditions were estimated using time-average.

2. Simulations were then performed at the same temperature (300 K) at different tensile uniaxial strains of 0% to 11.7505% in the NVT ensemble. The deformed supercell at each strain-level was relaxed using $0.5\text{x}10^6$ time-steps with a time period of 1 fs (the number of time-steps used was found to achieve converged results). The strain measure used is the Green strain given as $\varepsilon_{ij} = \frac{1}{2}\left(F_{ki}F_{kj} - \delta_{ij}\right)$. The lateral strains $\varepsilon_{22} = \varepsilon_{33} = 0$ and the shear strains $\varepsilon_{12} = \varepsilon_{23} = \varepsilon_{31} = 0$. The strain ε_{11} was applied along the [100] crystallographic direction (x axis or 1 direction) and the corresponding deformed edge vectors of the simulation box were computed for each axial strain. The position of every atom was recorded at every time-step of the simulation. In addition, the second moments, β_{ij}^{ab}, were computed at each atom with respect to itself and all its 999 neighbors.

3. For simulation at each strain-level, the atomic average $\beta_{ij}^{0b} = \frac{1}{N}\sum_{a=1}^{N}\beta_{ij}^{ab}$ over all the atoms was computed using an additional $2.0\text{x}10^6$ time-steps beyond convergence.

4. Each of the relaxed strained system at 300 K from step 2 was then quenched to ~0 K in the NVT ensemble. A quadratic polynomial

$$\bar{\phi} = A + Br_i^a + Cr_j^b + Dr_i^a r_j^b + E\left(r_i^a\right)^2 + F\left(r_j^b\right)^2$$

was fit to the resultant potential energy surface for perturbations of atoms a and b in the range of -0.05 Å to +0.05 Å, Subsequently, the zero temperature force constants, $k_{ij}^{ab,0}$, were computed at 5 representative atoms which were sufficiently far from the boundaries of the simulation box. Stiffness tensors including the self-

interaction as well as the 78 nearest neighbor interactions (b = 0 to 78) were computed.

5. The virial stress values at each strain at 300 K were calculated using the LAMMPS "compute stress per atom" command, summed over all atoms, and averaged over an additional 0.5×10^6 time-steps beyond convergence. The computed virial Cauchy stress is then transformed to the virial Piola stress denoted in the subsequent discussion as P_{ij}^{Virial}.

   The term $\frac{1}{V^0}\left(-\overline{f}_i^{\text{int},a}\overline{R}_j^a\right)$ in Eq.(16) was approximated using the "compute stress/atom" command in LAMMPS at 0 K and summing up the per-atom stress over all atoms and appropriately normalizing with the system volume.

3.2. Phonon frequencies and total stiffness tensor calculations

The phonon frequencies of a periodic crystal can be calculated using several different approaches (41,70,71). Here, we employ the method by Kong (70), in which the phonon frequencies can be directly computed from MD trajectories. For a pure crystal whose primitive cell consists of a single atom, the Green's functions in reciprocal space can be written in the form (see Appendix C):

$$\overset{\circ}{G}_{ij}\left(\overset{\mathrm{r}}{q}\right)=\frac{1}{N}\sum_{a,b}\beta_{ij}^{ab}e^{-i\overset{\mathrm{r}}{q}\cdot\left(\overset{\mathrm{r}}{r}^a-\overset{\mathrm{r}}{r}^b\right)} \tag{18}$$

Where N is the number of atoms in the supercell and $\overset{\mathrm{r}}{q}$ is the wavevector. Clearly, the Green's functions in reciprocal space are the forward Fourier transformations of the second moments, β_{ij}^{ab}, about equilibrium atomic positions. Under conditions where every atom is identical in a periodic lattice, Eq. (18) reduces to

$$\overline{\overline{G}}_{ij}\left(\vec{q}\right)=\sum_{b}\beta_{ij}^{0b}e^{-i\vec{q}\cdot\left(\vec{r}^{0}-\vec{r}^{b}\right)},$$

where $\beta_{ij}^{0b}=\frac{1}{N}\sum_{a=1}^{N}\beta_{ij}^{ab}$ is the atomic average of the second moments between an atom and its b^{th} neighbor.

The Fourier transform of the force constant matrix is obtained from the reciprocal space Green's function as $\overline{\overline{k}}_{ij}\left(\vec{q}\right)=k_{B}T\left[\overline{\overline{G}}^{-1}{}_{ij}\left(\vec{q}\right)\right]$, from which the dynamical matrix is obtained as $D_{ij}\left(\vec{q}\right)=\frac{1}{m}\overline{\overline{k}}_{ij}\left(\vec{q}\right)$, whose eigenvalues are the phonon frequencies ω_{i}. The inverse Fourier transform of $\overline{\overline{k}}_{ij}\left(\vec{q}\right)$ are used to calculate the finite temperature force constants $k_{ij}^{ab,T}$.

3.3. Local deformation gradient calculations

The deformation gradient at the site of each atom was calculated by minimizing the following sum of the squared error using the approach and weight functions proposed by Gullet et al. (31)

$$e^{m}=\sum_{n=1}^{N}\left(\Delta x_{i}^{mn}-F_{ij}^{m}\Delta X_{j}^{mn}\right)\left(\Delta x_{i}^{mn}-F_{ik}^{m}\Delta X_{k}^{mn}\right)w^{n} \tag{19}$$

Where e^{m} is the weighted error in position of atom m, Δx_{i}^{mn} is the vector from the mean position of atom m to the mean position of atom n in the deformed configuration, ΔX_{j}^{mn} is the same vector in the undeformed configuration, F_{ij}^{m} is the deformation gradient at the site of atom m, and w^{n} are the weight functions used to weight the error contribution for the atomic pair (m,n). The weight functions are inversely proportional to the distance

between atoms m and n. The cut-off radius proposed by Gullet et al. (31) is assigned based on the spread of β_{ij}^{0b} (the implementation is discussed later in sections 4.1 and 4.5).

4. Results and discussion

In the discussion of the results, the kinematics of deformation is described at 300 K, while for the discussion of stress; results are also presented at 750 K to highlight the contribution of the vibration stress to the free energy of deformation.

4.1. Validation of MD simulations

Figure 1 shows the phonon dispersion at 0% strain obtained from the second moments about equilibrium atomic position using the procedure described in section 3.3. The predictions closely match the trend of the experimental data (72) for the phonon dispersion curves validating the second moment calculations. We note that the magnitudes of the computed frequencies are somewhat smaller than the experimental values since our simulation is at 300 K, while the experimental data (72) was measured at 80 K.

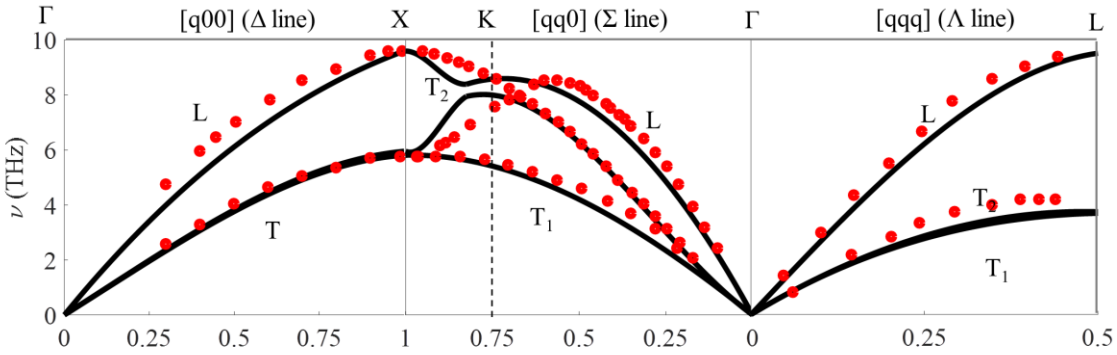

Figure 1 Phonon dispersion curves computed from the second moments about equilibrium atomic position

4.2. Adequacy of quasi-harmonic approximation

The percent difference between the terms $\left\langle \phi^{\text{int}} \right\rangle - \bar{\phi}^{\text{int}}$ and $\sum_{a=1}^{N}\sum_{b=1}^{N} k_{ij}^{\text{int},ab}\beta_{ij}^{ab}$ provides an indication of the adequacy of the quasi-harmonic approximation of the internal potential as shown in Figure 2, where $\bar{\phi}^{\text{int}}$ refers to the internal energy of the system with all the atoms fixed at their equilibrium positions. $\sum_{a=1}^{N}\sum_{b=1}^{N} k_{ij}^{ab,0}\beta_{ij}^{ab}$ is the vibrational part of the potential energy resulting from a zero temperature estimation of the force constants. It is seen that the error in energy estimation contributed by $\sum_{a=1}^{N}\sum_{b=1}^{N} k_{ij}^{ab,0}\beta_{ij}^{ab}$ is positive and increases with deformation from 5.0% to 17.7%. Accounting for finite temperature using $\sum_{a=1}^{N}\sum_{b=1}^{N} k_{ij}^{ab,T}\beta_{ij}^{ab}$ brings down the error, which varies from -2.6% to -4.7% under deformation. It is interesting to see that using $k_{ij}^{\text{int},ab} = k_{ij}^{ab,0}$, the total potential energy is overestimated if only the contribution from the zero temperature force constants is considered, while use of the finite temperature force constants underestimates the total potential energy. The implications on the stress calculation are discussed in section 4.4.

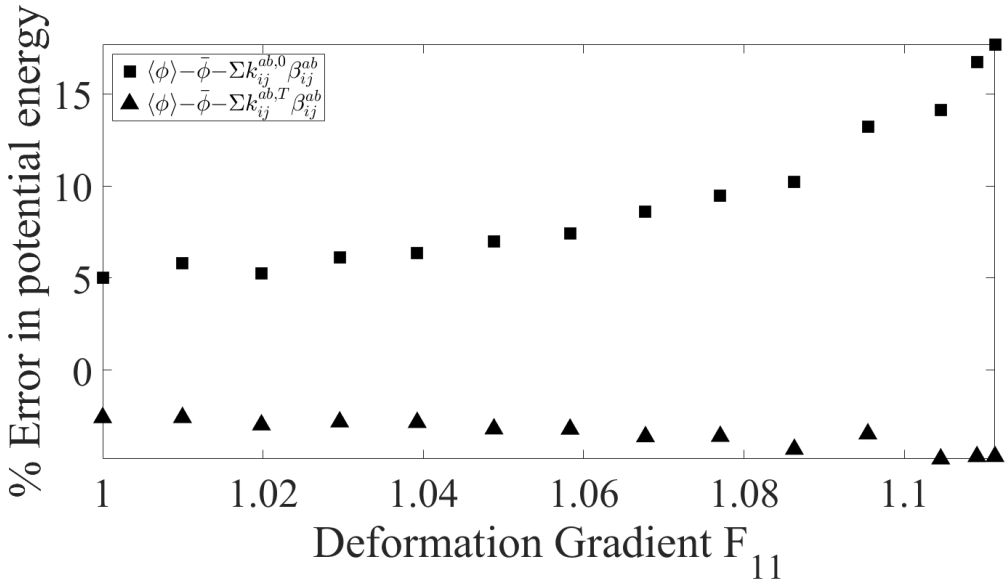

Figure 2 Percentage error in quasi-harmonic approximation versus continuum scale deformation gradient

4.3. Variation in the second moments with loading

Figure 3(a) shows the variation of the atomic average of the self-interaction second moments of atoms about equilibrium position, that is $\beta_{ii}^{00} = \frac{1}{N}\sum_{pp=1}^{N} \beta_{ii}^{pp}$ (where N is the number of atoms and no summation on repeated index i is imposed), with applied deformation gradient. As expected, the value of β_{ii}^{00} is isotropic at 0% strain. We observe that as the applied tensile strain increases, the second moment becomes anisotropic and has higher amplitude in the direction of loading. Further, we observe that the change is solely due to deformation of the system since the temperature is kept constant.

We note here that the introduced method in section 2.2 does not require the postulation of generator functions as in some other attempts (21,22). As discussed in Appendix A, unique and general generator function for canonical ensemble may not be easily obtained. For generator functions that lead to affine transformations of trajectories, the second moment takes the form $\beta_{ij}^{ab} = F_{im}F_{jk}\mathrm{B}_{mk}^{ab}$, where B_{mk}^{ab} are the second moments before deformation. The second moments for this case are also shown in Figure 3(a). The variation of mean square displacement β_{ii}^{00} from the MD simulation is clearly significantly different compared to that from the generator function. Remarkably, the affine mapping approach predicts no change in β_{22}^{00} and β_{33}^{00} with loading, which is clear contrast to that in the MD simulation. To further illustrate these differences, in Figure 3(b) we plot the atom-wise maps of the 11 component of the vibration tensors obtained

from the affine mapping approach and the MD simulations at 11.7505% strain. The atom-wise map of F_{11}^{a} used to calculate $G_{11}^{aa,affine}$ is also shown in Figure 3(b). We observe a remarkable difference in the vibration tensor calculated in the MD simulations versus that obtained as a consequence of affine mapping assumption applied locally to each atom. We remark that the transition from affine to non-affine displacements of atomic equilibrium position takes place between 11.75% and 11.7505% strain. In addition, we note that the histogram of F_{11}^{a} still retains some resemblance to a bell-curve and $G_{11}^{aa,affine}$ is still normally distributed, while the histogram of $G_{11}^{aa,MD}$ has completely deviated from a normal distribution. We further observe that in transitioning through the softening regime, the local values of $G_{11}^{aa,MD}$ at the site of atoms in the region of localized non-affine deformation undergo an increase several times larger than $G_{11}^{aa,affine}$. These observed discrepancies emphasize the need for additional local kinematic descriptors that can capture the effect of evolving vibrations under deformation. Some researchers (51,52) have pointed out that thermal vibrations can cause non-affine displacements even in a homogeneous crystal, leading to fluctuation-driven instability. Further, we note that the change in β_{ii}^{00} with strain is non-linear and is well-fit (R^2=0.999) using a cubic curve.

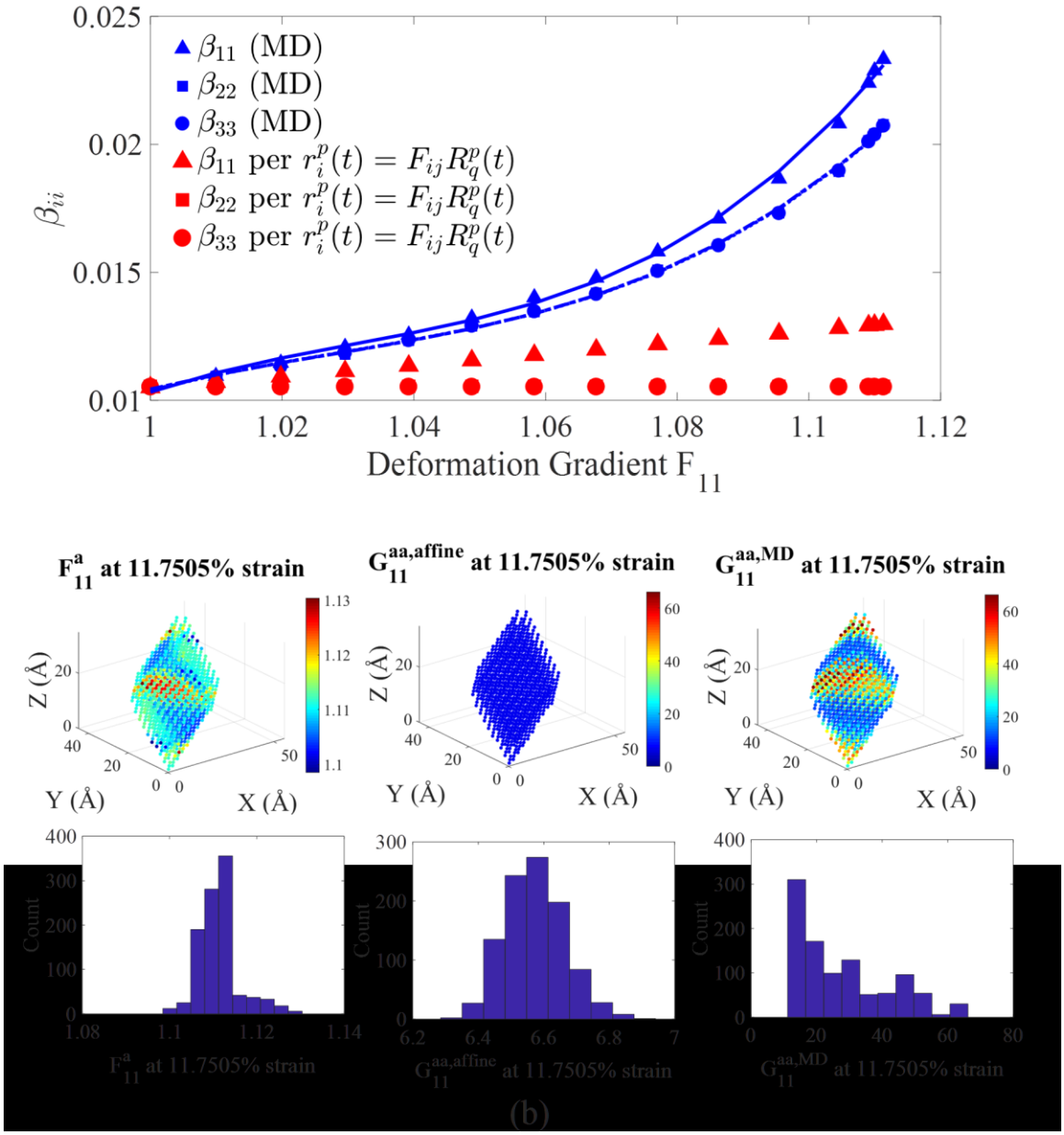

Figure 3 (a) Variation in second moments with continuum scale deformation gradient: comparison of observations from MD with those computed using F as the trajectory-to-trajectory mapping function, and (b) Atom-wise maps and histograms for 11 component of local deformation gradients and vibration tensors at 11.7505% strain obtained from affine transformations and the MD simulations.

Figure 4(a), (b) and (c) show that the inter-atomic second moments β_{11}^{0b}, β_{22}^{0b} and β_{33}^{0b} all increase non-linearly with applied strain for all the first 12 nearest neighbors (b = 1 to 12). For β_{11}^{0b}, the increase in the neighbors lying in the (010) and (001) crystallographic

planes (yx and xz Cartesian planes) is similar, and greater than those lying in the (100) plane (yz plane). The values of β_{11}^{0b} are significantly different from those predicted by an affine trajectory transform. For β_{22}^{0b} and β_{33}^{0b}, the largest values are for the neighbors lying in the (100) plane (yz plane) followed by those in the (010) and (001) (xy and xz) planes. It is interesting that the affine transformation does not predict a change in the interatomic second moments β_{22}^{0b} and β_{33}^{0b} with applied deformation, while the results from the MD simulation show a significant change. Figure 4(d) shows the variation in the off-diagonal β_{ij}^{0b} values with deformation gradient. Notably, the β_{12}^{0b}, β_{23}^{0b} and β_{13}^{0b} values are only significant for the neighbors in the (001) (xy), (100) (yz) and (010) (xz) planes. Figure 4(d) also shows that the off-diagonal β_{ij}^{0b} values change more significantly for the 23 components as compared to 12 and 13 components. The minimal change in the 12 and 13 components agrees with the prediction of the affine mapping approach. However, for the 23 components the affine approach is completely incorrect. All the changes in inter-atomic second moments follow the symmetry break due to the strain applied along the [100] direction. Overall, it is clear that application of strain reduces the crystal symmetry, and affects the local potential landscape, which leads to the observed trends in β_{ij}^{0b}. The underlying reason for the inconsistency between the second moments predicted by the simulation and by the affine mapping approach is that the affine approach does not account for the local changes in potential landscape.

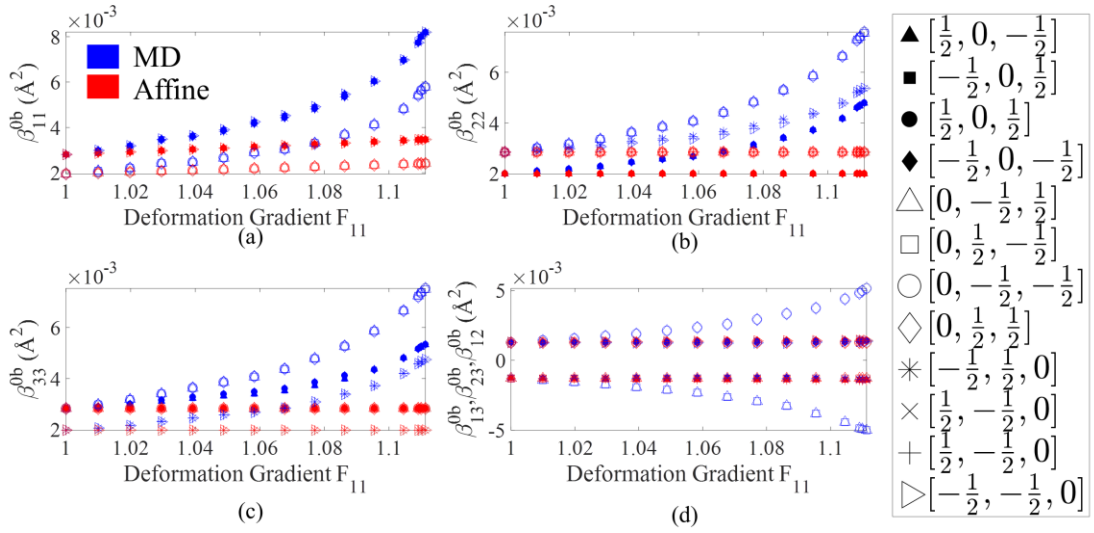

Figure 4 Variation in β_{ij}^{0b} for the first 12 nearest neighbors

4.4. Finite temperature stress

Figure 5(a) shows a plot of the static stress P_{11}^{T}, vibration stress P_{11}^{Q}, total Piola stress P_{11} in the 1-direction, computed using Eqs. (16), (17) and (15) respectively, and P_{11}^{Virial} obtained from LAMMPS, plotted against the deformation gradient at two temperatures of 300 K and 750 K. We find that $P_{11}^{Virial} > P_{11}^{T} > P_{11}$, however the difference between P_{11}^{T}, P_{11}^{Virial} and P_{11} is minimal at 300 K, and the magnitude of the vibration stress P_{11}^{Q} is only about 3% that of P_{11}. The agreement is interesting, given the difference in stress calculation procedures; while the stress in LAMMPS is derived from kinetic and potential contributions using the affine trajectory transformation, the stress we derive in section 2.2 is based on work done under a quasi-static deformation. At the higher temperature of 750 K, P_{11} is about 40% lower than P_{11}^{Virial} at 8% tensile strain; the magnitude of the vibration stress P_{11}^{Q} is about 27% of the magnitude of P_{11}. The agreement at 300 K appears to be

purely coincidental and further examination for complex systems is needed to verify its generality.

It is notable that P_{11}^{Virial} can be shown to be the exact work conjugate of the deformation gradient under the assumption that a canonical transform generator function, causing an affine transformation of thermal trajectories, holds true (22). Further, we note that in the case where this assumption does not hold, P_{11}^{Virial} does not completely capture the free energy change. Therefore, the differences between P_{11} and P_{11}^{Virial}, as well as the significance of P_{11}^{Q} can be related to the deviation of β_{ii}^{00} from affine behavior, discussed in section 4.3. The affine transformation of trajectories under-predicts the contribution of thermal vibration and thus over-predicts the stress. Observing the results described in section 4.2, it is likely that a more exact estimate of the stress lies between P_{11} and P_{11}^{T}.

At low strain-levels and low temperatures, the vibration stress can be assumed to be insignificant; however at high temperatures and high strains, the vibration stress increases to significant levels, steeply increasing in magnitude as the strain nears the softening point. On a related note, it has been suggested that elastic instability may be preceded by instabilities in vibration modes driven by thermal fluctuations (51,52,73). As discussed earlier (section 2.3), the stress calculation in classical MD approaches, such as LAMMPS, includes a kinetic contribution that has resemblance with the 2nd term of Eq. (16) and in Figure 5(b) we compare the two. While the kinetic contribution marginally decreases in magnitude in a linear manner over the loading regime, the 2nd term of Eq. (16) that involves the vibration tensor evolves significantly, and nonlinearly, with strains. The linear decrease of the kinetic contribution is entirely due to the volume change since

the $\left\langle v_i^a v_i^a \right\rangle$ terms do not change at constant temperature. The nonlinearity in the 2nd term of Eq. (16) is likely due to the anharmonicity of the EAM potential used to describe aluminum. In the virial stress formulation, this nonlinearity is embedded into the potential part of the stress, but its contribution to the free energy is underestimated due to the affine transformation approximation on the atomic trajectories. The comparisons in Figures 5(a) and 5(b) show the need for additional kinematic descriptors that can capture the effect of evolving vibrations under deformation.

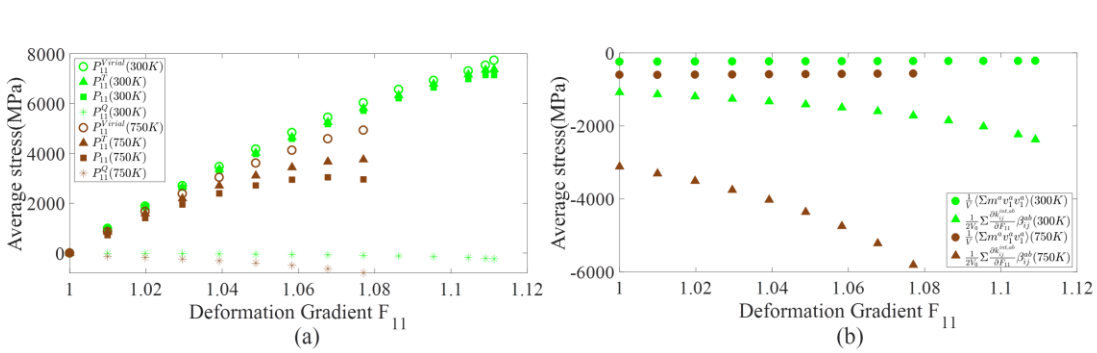

Figure 5 (a) Average Piola stress (static, vibration and LAMMPS) versus deformation gradient, and (b) Kinetic/vibration contribution to static stress.

4.5. Variation in directionality of second moments in peak stress vicinity

Figure 6 shows the atom-wise distribution of the direction cosines of the primary eigenvectors of F_{11}^a and G_{11}^a across the supercell at ε_{11} = 11.75% and ε_{11} = 11.7505%, which corresponds to peak value of P_{11}^{Virial}. The transition from affine to non-affine displacements of atomic equilibrium positions takes place between these two strain values. Figures 6(a) and (b) shows that the primary eigenvectors of the local deformation gradients continue to point in the [100] direction (loading direction) on either side of the softening peak. Comparison between Figures 6(c) and (d) show that the primary

eigenvectors of G_{11}^{aa} at ε_{11} = 11.7505% strongly deviate from the loading direction in the softening region, as compared to ε_{11} = 11.75%. This indicates that the "atomic clouds" formed by the trajectories have rotated away in this region from the direction of loading. This effect is similar to the rotational degree-of-freedom envisaged in micropolar continuum theory thus pointing to the need for enhanced continuum models for properly describing failure of even such simple material systems.

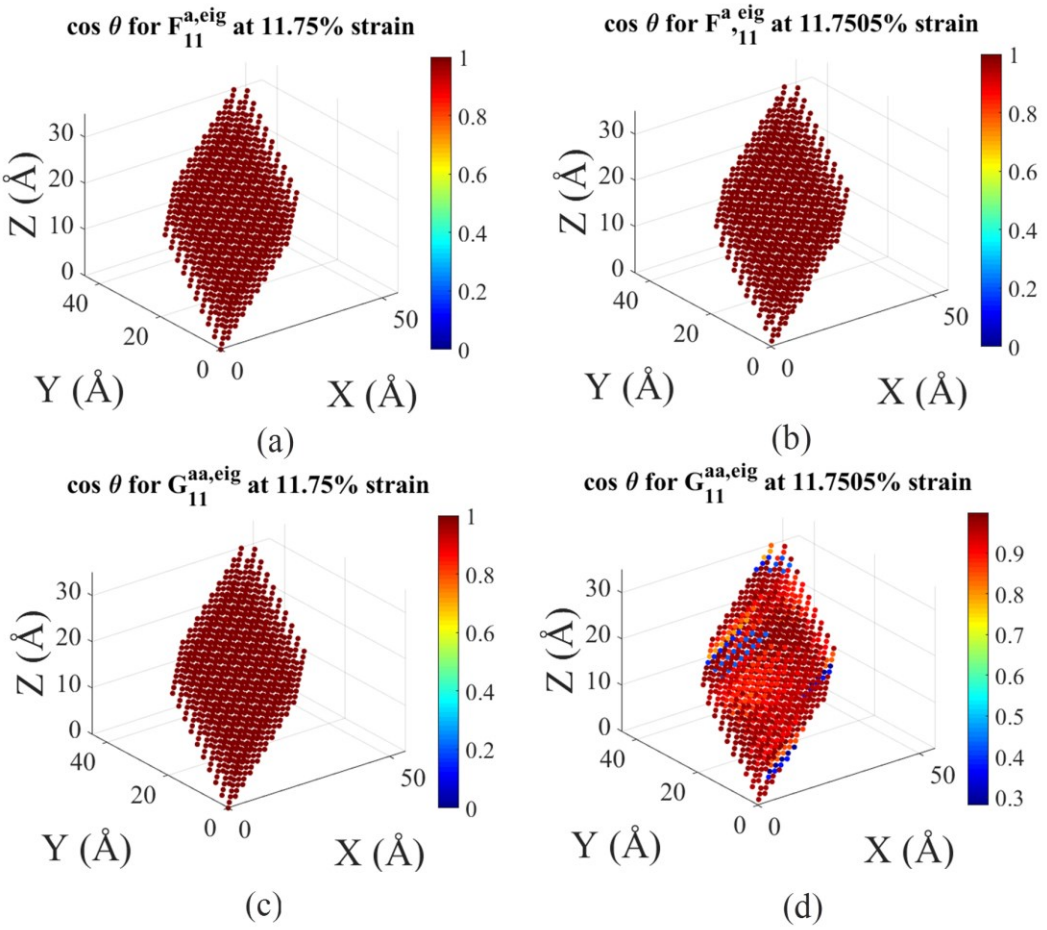

Figure 6 (a) Atom-wise map of direction cosine of primary eigenvector of vibration tensor at 11.75% strain (b) Atom-wise map of direction cosine of primary eigenvector of deformation gradient at 11.7505% strain (c) Atom-wise map of direction cosine of primary eigenvector of vibration tensor at 11.75% strain (d) Atom-wise map of primary eigenvector of vibration tensor at 11.7505% strain

4.6. Potential wells at incipient plasticity

To provide a vivid visualization of the "atomic clouds", Figure 7(a) shows the trajectory and probability density at every point of the trajectory for a sample atom in the softening region at 11.7505% strain. Figure 7(b) shows that this atom is oscillating between two potential wells leading to an asymmetric dumbbell shaped "atomic cloud". The geometric centers of each of the two spheres of the dumbbell are shown in Figure 7(c) indicated by large red circles. The deviation in the equilibrium position of the sample atom from the Cauchy-Born rule is only 0.026 Å. However, the distance between the centers of the ellipses of the dumbbell is about 1.8 Å. Correspondingly, in Figure 7(b), we observe the distance between the minima of the potential wells to be close to 1.8 Å. Although the atom resides close to its equilibrium position for a majority of the time, the second cloud is considerably displaced from the initial position and has entered the octahedral interstitial site shown in Figure 7(c). The change in second moment about equilibrium position for this atom is 0.043 $Å^2$. We note that the second moment is insufficient to model such a change in shape of the atomic trajectory cloud; however, the use of a spherical harmonic expansion, as used in atomic orbitals, can potentially capture such changes. In any case, the softening of the material corresponds to the jump of the atom from the deeper potential well to the shallower one. We conjecture that the onset of such a transition will be characterized by a critical value of G_{11}^{aa}. The existence of such a condition may provide additional criterion for the formulation of finite-temperature continuum plasticity theory and needs further investigations.

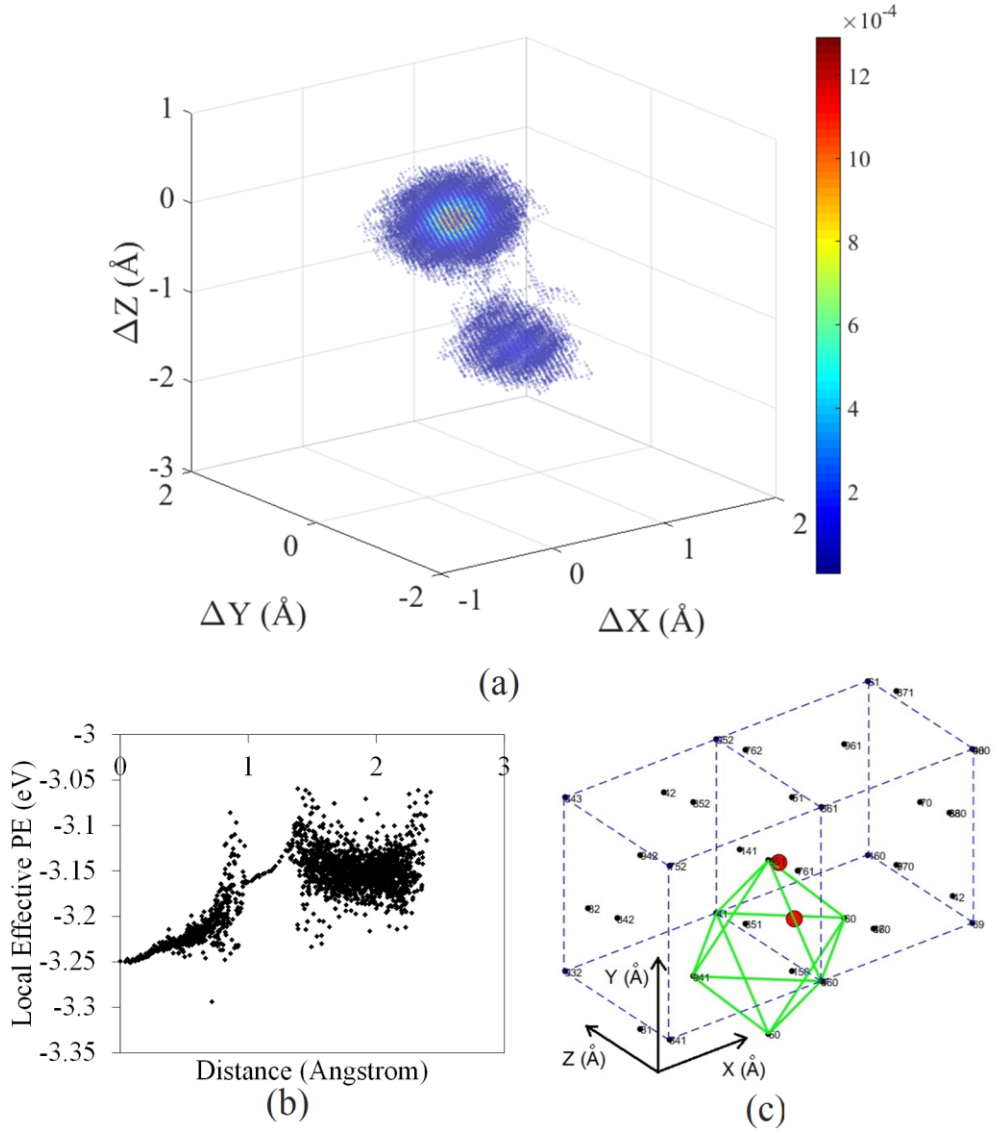

Figure 7 (a) Dumbbell shaped cloud of atomic trajectory along with probability density at each location for sample atom in region of failure, (b) Potential energy well(s) for sample atom (c) centers of the ellipses of the dumbbell shaped cloud

5. Concluding Remarks and Epilogic Discussion

In this paper, we have shown that the stress-strain conjugate pair formed by the static component of the Piola stress and deformation gradient only captures the changes in the potential energy landscape that are result of change in equilibrium atomic positions, but

does not capture changes in the local potential energy landscapes which are a result of thermal vibration evolution with deformation. On the other hand, the vibration stress and the vibration component of the Piola stress that we have derived in this paper capture part of the changes in the local potential energy landscapes caused by the evolution of thermal vibration of atoms under macroscopic deformation. Therefore, they promise to be useful continuum measures to extract from finite temperature molecular simulations. While stress conjugates to non-affine fields caused by structural disorder have been derived in a discrete-to-continuum setting using micromorphic (11,74,75) or strain-gradient methods (48,49,76,77), stress conjugates to real-space kinematic fields resulting from non-affine thermal vibration have not been explicitly derived, even though the mechanical importance of considering non-affinity from thermal vibration has been recognized in recent times (50–52). Our simulations show that the contribution of non-affine evolution of thermal vibrations to the free energy change can be significant even for the case of statically homogeneous deformation of an ordered crystalline solid such as fcc Aluminum with only a single atom in the primitive unit cell. The vibration stress and vibration tensor are expected to play a more significant role for solids with a more complex structure than fcc aluminum. In summary, we have:

(a) analyzed some of the nuances of the virial stress derivation which use the deformation gradient to map deformed and undeformed trajectories,

(b) shown that the canonical transform assumption used for trajectory mapping does not always hold in NVT ensembles by tracking the change in second moments about equilibrium positions under uniaxial deformation of fcc aluminum,

(c) provided an alternative method for computing local deformation measures and their conjugate stresses at atomic sites, under the condition of quasi-static deformation, by decomposing the change in atomic trajectory into deformation gradient and vibration tensor, and

(d) demonstrated the relevance of the vibration stress and vibration tensor to incipient plasticity in the material. We elaborate the highlights of our findings in the following sections.

5.1. Relevance of our formalism to continuum scale kinematic variables

Possible choices that have been used for continuum scale kinematic variables include combination of deformation gradient with temperature (F, T) or with entropy (F, S). In this paper, we have demonstrated that the deformation gradient and vibration tensor pair (F, G) is a particularly useful kinematic variable set for continuum interpretations of atomistic models at finite temperature. It simplifies work conjugacy at the atomic scale and is a suitable choice for localization frameworks where high spatial resolution, approaching the atomic scale, is required without simultaneous need for high temporal resolution. Furthermore, it could be used to develop atomistically motivated finite temperature failure theories based on molecular dynamics or other discrete simulations. For example, the elastic-plastic transition of single crystal platinum has been experimentally studied using nano-indentation and the authors have proposed that energy barriers for yield have a complex dependence on stress and temperature, and are eventually overcome by a combination of thermal and mechanical energies, under an appropriate thermal fluctuation (53). Since thermal trajectory evolution is built into our approach, formulation of continuum theories to describe such phenomena may prove to

be easier in a *(F, G)* framework as opposed to a *(F, T)* or *(F, S)* framework. Moreover, local representations of temperature are not required in this proposed formulation.

5.2. Relevance of our formalism to failure theories

The appearance of non-affine deformation regions are being utilized to detect regions of failure (1). The appearance of imaginary frequencies in the phonon dispersion is also used to identify mechanical instability (78). It has been known for several decades that the presence of a critical r.m.s atomic vibration amplitude or a critical amount of "free volume" at the dislocation in a crystal is strongly correlated to the beginning of plastic flow associated with a localized "melting" (79). More recently, a "hidden" critical point which is related to percolation thermally induced non-affine droplets has been observed in the pre-yield strain regime of a crystalline solid using MD simulation (80). In this context, the vibration tensor and similar higher moment measures could serve as deformation measures with high sensitivity to unveil and predict the onset of material instability, particularly at high temperatures. Recent research has shown the instability of phonon lattice dynamics calculations in the neighborhood of failure for Aluminum-Titanium alloys using the lattice dynamical finite element method (LDFEM) (81). The LDFEM method explicitly separates stress calculation into (a) stress at zero temperature and (b) instabilities studied by using phonon dispersion spectra. We suggest that the use of presented formalism in place of the phonon gas approach will ensure that the corresponding deformation fields along with their stress conjugates are all in the real space and may be input into a larger-scale FE simulation with (F,G) as kinematic deformation fields. The use of real space makes our approach attractive to amorphous solids. The incorporation of higher orders of vibration in addition to G can enrich

continuum models even more, making it possible to include changes in the shape of the trajectory cloud. Particularly, as presented in section 4.6, the probability density of the atomic position may be described to be undergoing a smooth transition from an ellipse to a dumbbell. The presented approach can be extended to include such deformation by expanding the probability density of atomic position in suitable form such as spherical harmonics.

Acknowledgements

This research is supported in part by DOE Research Grant DE-NA0002630 (LO) and partly by United States National Science Foundation Grant CMMI-1727433 (AM). We also thank Drs. Sivapragasam Sathananthan and Sitaram Aryal from Tennessee State University for useful discussion regarding Fourier Transform and Python coding.

References

1. Hu YC, Guan PF, Li MZ, Liu CT, Yang Y, Bai HY, et al. Unveiling atomic-scale features of inherent heterogeneity in metallic glass by molecular dynamics simulations. Phys Rev B - Condens Matter Mater Phys. 2016;93(21).
2. Hong Z-H, Hwang S-F, Fang T-H. Atomic-level stress calculation and surface roughness of film deposition process using molecular dynamics simulation. Comput Mater Sci [Internet]. 2010;48(3):520–8. Available from: http://www.sciencedirect.com/science/article/pii/S0927025610000832
3. Egami T, Poon SJ, Zhang Z, Keppens V. Glass transition in metallic glasses: A microscopic model of topological fluctuations in the bonding network. Phys Rev B - Condens Matter Mater Phys. 2007;76(2).
4. Cheng YQ, Ma E. Atomic-level structure and structure-property relationship in metallic glasses. Prog Mater Sci. 2011;56(4):379–473.
5. Shiihara Y, Kohyama M, Ishibashi S. Ab initio local stress and its application to Al (111) surfaces. Phys Rev B. APS; 2010;81(7):75441.
6. Yang Z, Lu Z, Zhao Y-P. Shape effects on the yield stress and deformation of silicon nanowires: A molecular dynamics simulation. J Appl Phys. AIP; 2009;106(2):23537.
7. Zimmerman J a., Webb EB, Hoyt JJ, Jones RE, Klein P a., Bammann DJ. Calculation of stress in atomistic simulation. Model Simul INMATERIALS Sci Eng Model. 2004;12:S319–32.
8. Chang CS, Misra A. Packing structure and mechanical properties of granulates. J Eng Mech. 1990;116(5):1077–93.

9. Chang CS, Chao SJ, Chang Y. Estimates of elastic moduli for granular material with anisotropic random packing structure. Int J Solids Struct. 1995;32(14):1989–2008.
10. Misra A, Parthasarathy R, Ye Q, Singh V, Spencer P. Swelling equilibrium of dentin adhesive polymers formed on the water-adhesive phase boundary: Experiments and micromechanical model. Acta Biomater. 2014;10(1):330–42.
11. Misra A, Chang CS. Effective elastic moduli of heterogeneous granular solids. Int J Solids Struct. 1993;30(18):2547–66.
12. Misra A, Parthasarathy R, Singh V, Spencer P. Micro-poromechanics model of fluid-saturated chemically active fibrous media. ZAMM Zeitschrift fur Angew Math und Mech. Wiley-VCH Verlag; 2015;95(2):215–34.
13. Misra A, Singh V. Micromechanical model for viscoelastic materials undergoing damage. Contin Mech Thermodyn. Springer; 2013;25(2–4):343–58.
14. Misra A, Singh V. Thermomechanics-based nonlinear rate-dependent coupled damage-plasticity granular micromechanics model. Contin Mech Thermodyn. Springer; 2015;27(4–5):787–817.
15. Misra A, Poorsolhjouy P. Grain- and macro-scale kinematics for granular micromechanics based small deformation micromorphic continuum model. Mech Res Commun. 2017;81:1–6.
16. J. Clerk-Maxwell. Van der Waals and the continuity of the Gaseous and Liquid state. Nature. 1874;10:477–80.
17. Lutsko JF. Stress and elastic constants in anisotropic solids: Molecular dynamics techniques. J Appl Phys. 1988;64(3):1152–4.

18. Louwerse MJ, Baerends EJ. Calculation of pressure in case of periodic boundary conditions. Chem Phys Lett. 2006;421(1–3):138–41.

19. Liu B, Qiu X. How to compute the atomic stress objectively? J Comput Theor Nanosci. 2009;6(5):1081–9.

20. Jiang H, Huang Y, Hwang KC. A Finite-Temperature Continuum Theory Based on Interatomic Potentials. J Eng Mater Technol [Internet]. 2005;127(4):408–16. Available from: http://materialstechnology.asmedigitalcollection.asme.org/article.aspx?articleid=1427525

21. Admal NC, Tadmor EB. A unified interpretation of stress in molecular systems. J Elast. Springer; 2010;100(1):63–143.

22. Tadmor EB, Miller RE. Modeling materials: continuum, atomistic and multiscale techniques. Cambridge University Press; 2011.

23. Zhou M. A new look at the atomic level virial stress: on continuum-molecular system equivalence. Proc R Soc A Math Phys Eng Sci [Internet]. 2003;459(2037):2347–92. Available from: http://rspa.royalsocietypublishing.org/content/459/2037/2347.abstract

24. Tsai DH. The virial theorem and stress calculation in molecular dynamics. J Chem Phys [Internet]. 1979;70(3):1375. Available from: http://scitation.aip.org/content/aip/journal/jcp/70/3/10.1063/1.437577

25. Thompson AP, Plimpton SJ, Mattson W. General formulation of pressure and stress tensor for arbitrary many-body interaction potentials under periodic boundary conditions. J Chem Phys. 2009;131(15).

26. Subramaniyan AK, Sun CT. Continuum interpretation of virial stress in molecular simulations. Int J Solids Struct. 2008;45(14–15):4340–6.

27. Sunyk R, Steinmann P. On higher gradients in continuum-atomistic modelling. Int J Solids Struct. 2003;40(24):6877–96.

28. Nie XB, Chen SY, E WN, Robbins MO. A continuum and molecular dynamics hybrid method for micro- and nano-fluid flow. J Fluid Mech [Internet]. 2004;500(2004):55–64. Available from: http://www.journals.cambridge.org/abstract_S0022112003007225

29. Chen Y, Lee JD, Hardy RJ, Chen Y, Lee JD. Connecting molecular dynamics to micromorphic theory.(II). Balance laws. Phys A Stat Mech its Appl [Internet]. Elsevier; 2003;322(1):622. Available from: http://link.aip.org/link/?JCP/76/622/1&Agg=doi

30. Chen Y, Lee JD. Connecting molecular dynamics to micromorphic theory. (I). Instantaneous and averaged mechanical variables. Phys A Stat Mech its Appl. 2003;322:359–76.

31. Gullett PM, Horstemeyer MF, Baskes MI, Fang H. A deformation gradient tensor and strain tensors for atomistic simulations. Model Simul Mater Sci Eng [Internet]. 2008;16(1):015001. Available from: http://stacks.iop.org/0965-0393/16/i=1/a=015001?key=crossref.8abcd921806ae8572e08fc13246555fa

32. Hardy RJ. Formulas for determining local properties in molecular-dynamics simulations: Shock waves. J Chem Phys [Internet]. 1982;76(1):622. Available from: http://link.aip.org/link/?JCP/76/622/1&Agg=doi

33. Irving JH, Kirkwood JG. The Statistical Mechanical Theory of Transport

Processes. IV. The Equations of Hydrodynamics. J Chem Phys [Internet]. 1950;18(6):817. Available from: http://scitation.aip.org/content/aip/journal/jcp/18/6/10.1063/1.1747782

34. Lee JD, Chen Y, Wang X. Extending micromorphic theory to atomic scale. In: Mechanics of Generalized Continua. Springer; 2010. p. 109–17.
35. Zimmerman JA, Bammann DJ, Gao H. Deformation gradients for continuum mechanical analysis of atomistic simulations. Int J Solids Struct. 2009;46(2):238–53.
36. Zimmerman JA, Jones RE, Templeton JA. A material frame approach for evaluating continuum variables in atomistic simulations. J Comput Phys. 2010;229(6):2364–89.
37. Hardy RJ, Root S, Swanson DR. Continuum properties from molecular simulations. In: AIP Conference Proceedings. 2002. p. 363–6.
38. Kuzkin VA, Krivtsov AM, Jones RE, Zimmerman JA. Material frame representation of equivalent stress tensor for discrete solids. Phys Mesomech. Springer; 2015;18(1):13–23.
39. Krivtsov AM, Kuz'kin VA. Derivation of equations of state for ideal crystals of simple structure. Mech solids. Springer; 2011;46(3):387.
40. Admal NC, Tadmor EB. Material fields in atomistics as pull-backs of spatial distributions. J Mech Phys Solids. Elsevier; 2016;89:59–76.
41. Weiner JH. Statistical mechanics of elasticity. Courier Corporation; 2012.
42. Panchenko AY, Podolskaya EA, Krivtsov AM. Analysis of equations of state and determination of the Grüneisen function for two-dimensional crystal lattices. In:

Doklady Physics. 2017. p. 141–4.

43. Kuzkin VA, Krivtsov AM. Nonlinear positive/negative thermal expansion and equations of state of a chain with longitudinal and transverse vibrations. Phys status solidi. Wiley Online Library; 2015;252(7):1664–70.

44. Kuzkin VA, Krivtsov AM. An analytical description of transient thermal processes in harmonic crystals. Phys Solid State. Springer; 2017;59(5):1051–62.

45. Krivtsov AM, Kuzkin VA. Discrete and Continuum Thermomechanics. arXiv Prepr arXiv170709510. 2017;

46. Chen Y, Lee JD. Connecting molecular dynamics to micromorphic theory.(II). Balance laws. Phys A Stat Mech its Appl. Elsevier; 2003;322:377–92.

47. Cheung KS, Yip S. Atomic-level stress in an inhomogeneous system. J Appl Phys. AIP; 1991;70(10):5688–90.

48. Admal NC, Marian J, Po G. The atomistic representation of first strain-gradient elastic tensors. J Mech Phys Solids. Elsevier; 2017;99:93–115.

49. Arndt M, Griebel M. Derivation of Higher Order Gradient Continuum Models from Atomistic Models for Crystalline Solids [Internet]. Multiscale Modeling & Simulation. 2005. 531-562 p. Available from: http://epubs.siam.org/doi/10.1137/040608738

50. Ganguly S, Mohanty PS, Schurtenberger P, Sengupta S, Yethiraj A. Contrasting the dynamics of elastic and non-elastic deformations across an experimental colloidal Martensitic transition. Soft Matter [Internet]. 2017;1–7. Available from: http://arxiv.org/abs/1705.00741

51. Ganguly S, Sengupta S. Excess vibrational modes of a crystal in an external non-

affine field. J Chem Sci. Springer; 2017;129(7):891–7.

52. Ganguly S, Sengupta S, Sollich P, Rao M. Nonaffine displacements in crystalline solids in the harmonic limit. Phys Rev E. APS; 2013;87(4):42801.

53. Mason JK, Lund AC, Schuh CA. Determining the activation energy and volume for the onset of plasticity during nanoindentation. Phys Rev B - Condens Matter Mater Phys. 2006;73(5).

54. Ketov S V., Sun YH, Nachum S, Lu Z, Checchi A, Beraldin AR, et al. Rejuvenation of metallic glasses by non-affine thermal strain. Nature. 2015;524(7564):200–3.

55. Kassner ME, Smith K. Low temperature creep plasticity. J Mater Res Technol. Elsevier; 2014;3(3):280–8.

56. Mukherjee AK, Bird JE, Dorn JE. Experimental correlations for high-temperature creep. 1968;

57. Startsev VI. Low temperature creep of metals. Czechoslov J Phys. Springer; 1981;31(2):115–24.

58. Komarasamy M, Kumar N, Mishra RS, Liaw PK. Anomalies in the deformation mechanism and kinetics of coarse-grained high entropy alloy. Mater Sci Eng A. 2016;654:256–63.

59. Rehage G. Elastic properties of crosslinked polymers. Pure Appl Chem. 1974;39(1–2):161–78.

60. Flory PJ, Rehner Jr J. Statistical mechanics of cross-linked polymer networks I. Rubberlike elasticity. J Chem Phys. AIP; 1943;11(11):512–20.

61. Lappala A, Zaccone A, Terentjev EM. Polymer glass transition occurs at the

marginal rigidity point with connectivity z*= 4. Soft Matter. Royal Society of Chemistry; 2016;12(35):7330–7.

62. Argon AS. A theory for the low-temperature plastic deformation of glassy polymers. Philos Mag. Taylor & Francis; 1973;28(4):839–65.

63. Mulliken AD, Boyce MC. Mechanics of the rate-dependent elastic--plastic deformation of glassy polymers from low to high strain rates. Int J Solids Struct. Elsevier; 2006;43(5):1331–56.

64. Eyring H. Viscosity, plasticity, and diffusion as examples of absolute reaction rates. J Chem Phys. 1936;4:283.

65. Bauwens JC. Relation between the compression yield stress and the mechanical loss peak of bisphenol-A-polycarbonate in the β transition range. J Mater Sci. 1972;7(5):577–84.

66. Dell'Isola F, Andreaus U, Placidi L, Scerrato D. Intorno alle equazioni fondamentali del movimento di corpi qualsivogliono, considerati secondo la naturale loro forma e costituzione. In: The complete works of Gabrio Piola: Volume I. Springer; 2014. p. 1–370.

67. Zharkov VN, Kalinin VA. Equations of state for solids at high pressures and temperatures. Springer; 1971.

68. Plimpton S. Fast Parallel Algorithms for Short-Range Molecular Dynamics. J Comput Phys. 1995;117(1):1–19.

69. Daw MS, Baskes MI. Embedded-atom method: Derivation and application to impurities, surfaces, and other defects in metals. Phys Rev B. APS; 1984;29(12):6443.

70. Kong LT. Phonon dispersion measured directly from molecular dynamics simulations. Comput Phys Commun. Elsevier B.V.; 2011;182(10):2201–7.

71. Kong LT, Bartels G, Campañá C, Denniston C, Müser MH. Implementation of Green's function molecular dynamics: An extension to LAMMPS. Comput Phys Commun [Internet]. Elsevier B.V.; 2009;180(6):1004–10. Available from: http://dx.doi.org/10.1016/j.cpc.2008.12.035

72. Mishin Y, Farkas D, Mehl MJ, Papaconstantopoulos DA. Interatomic potentials for monoatomic metals from experimental data and ab initio calculations. Phys Rev B [Internet]. 1999;59(5):3393–407. Available from: http://link.aps.org/doi/10.1103/PhysRevB.59.3393%5Cnhttp://prb.aps.org/abstract/PRB/v59/i5/p3393_1%5Cnhttp://prb.aps.org/pdf/PRB/v59/i5/p3393_1

73. Clatterbuck DM, Krenn CR, Cohen ML, Morris Jr JW. Phonon instabilities and the ideal strength of aluminum. Phys Rev Lett. APS; 2003;91(13):135501.

74. Zaccone A, Scossa-Romano E. Approximate analytical description of the nonaffine response of amorphous solids. Phys Rev B. APS; 2011;83(18):184205.

75. Lemaitre A, Maloney C. Sum rules for the quasi-static and visco-elastic response of disordered solids at zero temperature. J Stat Phys. Springer; 2006;123(2):415.

76. Tarasov VE. Lattice model with nearest-neighbor and next-nearest-neighbor interactions for gradient elasticity. arXiv Prepr arXiv150303633. 2015;

77. Rosi G, Auffray N. Anisotropic and dispersive wave propagation within strain-gradient framework. Wave Motion. 2016;63:120–34.

78. Xiong K, Liu X, Gu J. Multiscale modeling of lattice dynamical instability in gamma-TiAl crystal. Model Simul Mater Sci Eng [Internet]. 2015;23(4):045006.

Available from: http://stacks.iop.org/0965-0393/23/i=4/a=045006?key=crossref.3fc0d0d11c1486177348034baac121d8

79. Gilman JJ. The plastic resistance of crystals. Aust J Phys. 1960;13:327.

80. Das T, Ganguly S, Sengupta S, Rao M. Pre-yield non-affine fluctuations and a hidden critical point in strained crystals. Sci Rep. Nature Publishing Group; 2015;5:10644.

81. Xiong K, Liu X, Gu J. Multiscale modeling of lattice dynamical instability in gamma-TiAl crystal. Model Simul Mater Sci Eng. IOP Publishing; 2015;23(4):45006.

82. Goldstein H, Poole CP, Safko J. Classical Mechanics. Massachusetts: Addison-Wesley; 1980.

83. Kong LT. Phonon dispersion measured directly from molecular dynamics simulations. Comput Phys Commun [Internet]. Elsevier B.V.; 2011;182(10):2201–7. Available from: http://dx.doi.org/10.1016/j.cpc.2011.04.019

Appendix A: Generator Function Approach

For a canonical ensemble, the modified Hamilton's principle states that:(21,22)

$$\delta\int_{t_1}^{t_2}\left(B_i^a\dot{R}_i^a - H(R_i^a, B_i^a, t)\right)dt = 0 \qquad \delta\int_{t_1}^{t_2}\left(p_i^a\dot{r}_i^a - \hat{H}(r_i^a, p_i^a, t)\right)dt = 0 \tag{A.1}$$

where $\left(R_i^a, B_i^a\right)$ are the position and momenta before deformation and $\left(r_i^a, p_i^a\right)$ are the position and momenta after deformation i.e. the transformation must maintain the Hamiltonian equations. $H(R_i^a, B_i^a, t)$ is the Hamiltonian function of the system before deformation and $\hat{H}(r_i^a, p_i^a, t)$ is the Hamiltonian function of the system after deformation. This pair of equations can only be satisfied under the following condition.

$$\left(p_i^a\dot{r}_i^a - \hat{H}(r_i^a, p_i^a, t)\right) + \frac{\mathrm{d}\Upsilon}{\mathrm{d}t} = B_i^a\dot{R}_i^a - H(R_i^a, B_i^a, t) \tag{A.2}$$

where Υ is the generator function which is an arbitrary scalar function of atomic position, momentum and time, and has continuous second derivatives(21,22). For example, the generator function may be assumed to be of the form: $\Upsilon = f_i^a\left(R_j^1, R_j^2 ....R_j^N, t\right)p_i^a - r_i^a p_i^a$ (82).

Substituting $\dfrac{\mathrm{d}\Upsilon}{\mathrm{d}t} = \left(\dfrac{\partial f_i^a}{\partial R_j^a}\dfrac{\partial R_j^a}{\partial t} + \dfrac{\partial f_i^a}{\partial t}\right)p_i^a + f_i^a\dot{p}_i^a - \dot{r}_i^a p_i^a - r_i^a\dot{p}_i^a$

in Eq. (A.2), we get:

$$\dot{p}_i^p\left(f_i^p - r_i^p\right) + \frac{\partial f_i^p}{\partial R_j^p}p_i^p\dot{R}_j^p - \hat{H}\left(r_i^p, p_i^p, t\right) + \dot{f}_i^p p_i^p = B_i^p\dot{R}_i^p - H\left(R_i^p, B_i^p, t\right)$$

Equating coefficients of each time derivative (or differential) term,

$$f_i^p - r_i^p = 0 \tag{A.3}$$

$$\frac{\partial f_j^p}{\partial R_i^p}p_j^p = B_i^p \tag{A.4}$$

$$\hat{H}\left(r_i^p, p_i^p, t\right) = H\left(R_i^p, B_i^p, t\right) + \dot{f}_i^p p_i^p \tag{A.5}$$

The above equations represent a one-to-one correspondence between the deformed and undeformed quantities which hold at any instant of time. Time averaging both sides of Eq. (A.5) gives insight into the nature of the generator function. The quantity $\left\langle \dot{f}_i^p p_i^p \right\rangle$ is the change in the total average energy of the system after deformation. From Eq. (A.5), f_i^p is the function that maps the trajectories from the undeformed configuration to the deformed configuration. When $\hat{H} = H$, it is possible to obtain generator functions which explicitly relate $\left(r_i^p, p_i^p\right)$ to $\left(R_i^p, B_i^p\right)$ (for example, see section 8.1.3, Tadmor and Miller(22)). However, for a canonical ensemble undergoing deformation under constant temperature, the condition $\hat{H} = H$ is not satisfied due to the requirement of constant temperature. Therefore, it is non-trivial to come up with a unique and general generator function in closed form for a canonical ensemble.

Appendix B: Derivation of the Virtual Work Expression

The total work done on the atom *a* (see Eq.(6)) is split into three parts δW^{a1}, δW^{a2} and δW^{a3}, defined as follows:

$$\delta W^{a1} = -\left\langle \overline{f}_i^{\text{int},a} \delta r_i^a \right\rangle \tag{B.1}$$

$$\delta W^{a2} = \left\langle \sum_b \left(k_{ij}^{\text{int},ab} - k_{ij}^{total,ab}\right)\left(r_j^b - \overline{r}_j^b\right)\delta r_i^a \right\rangle \tag{B.2}$$

$$\delta W^{a3} = \left\langle \frac{1}{2}\sum_c \sum_b \left.\frac{\partial k_{ij}^{\text{int},ab}}{\partial r_k^c}\right|_{r_k^c = \overline{r}_k^c} \left(r_j^b - \overline{r}_j^b\right)\left(r_k^c - \overline{r}_k^c\right)\delta r_i^a \right\rangle \tag{B.3}$$

Recognizing that the force on atom *a* at its equilibrium position, $\overline{f}_i^{\text{int},a}$, is independent of time, Eq. (B.1) is evaluated as follows:

$$\delta W^{a1} = -\overline{f}_i^{\text{int},a}\,\delta\overline{r}_i^{\,a} \tag{B.4}$$

where $\delta\overline{r}_i^{\,a}$ is the change in equilibrium position of atom *a*. In order to evaluate Eqs. (B.2) and (B.3), we use the fact that all the atoms in the supercell are equivalent in the range of study (0 to 11.75% strain). Using Eq. (B.2), we write the sum total of δW^{a2} over all the atoms, which we denote as δW^2, as follows:

$$\delta W^2 = \sum_a \left\langle \sum_b \left(k_{ij}^{\text{int},ab} - k_{ij}^{total,ab}\right)\left(r_j^b - \overline{r}_j^{\,b}\right)\delta r_i^a \right\rangle \tag{B.5}$$

We recognize that $k_{ij}^{\text{int},ab}$ and $k_{ij}^{total,ab}$ are evaluated at the equilibrium positions and therefore independent of time. With some rearrangement of terms, Eq. (B.5) is rewritten as:

$$\delta W^2 = \sum_a \sum_b \left(k_{ij}^{\text{int},ab} - k_{ij}^{total,ab}\right)\left(\left\langle \delta r_i^a r_j^b \right\rangle - \delta\overline{r}_i^{\,a}\overline{r}_j^{\,b}\right) \tag{B.6}$$

The first variation of $\beta_{ij}^{ab} = \left\langle r_i^a r_j^b \right\rangle - \overline{r}_i^{\,a}\overline{r}_j^{\,b}$ can be written as $\delta\beta_{ij}^{ab} = \delta\beta_{ij}^a + \delta\beta_{ij}^b$, where $\delta\beta_{ij}^a = \delta r_i^a r_j^b - \delta\overline{r}_i^{\,a}\overline{r}_j^{\,b}$ and $\delta\beta_{ij}^b = r_i^a \delta r_j^b - \overline{r}_i^{\,a}\delta\overline{r}_j^{\,b}$. Therefore, Eq. (B.6) is rewritten as follows

$$\delta W^2 = \sum_a \sum_b \left(k_{ij}^{\text{int},ab} - k_{ij}^{total,ab}\right)\left(\delta\beta_{ij}^a\right) \tag{B.7}$$

Since the stiffness tensors $k_{ij}^{\text{int},ab}$ and $k_{ij}^{total,ab}$ are symmetric,
$\delta W^2 = \sum_a \sum_b \left(k_{ij}^{\text{int},ab} - k_{ij}^{total,ab}\right)\left(\delta\beta_{ij}^b\right)$ also holds. Using $\delta\beta_{ij}^{ab} = \delta\beta_{ij}^a + \delta\beta_{ij}^b$, we can rewrite:

$$\delta W^2 = \frac{1}{2}\sum_a \sum_b \left(k_{ij}^{\text{int},ab} - k_{ij}^{total,ab}\right)\left(\delta\beta_{ij}^{ab}\right) \tag{B.8}$$

Writing the sum of δW^{a3} over all atoms, δW^3, and using the commutative property of $\frac{\partial k_{ij}^{\text{int},ab}}{\partial r_k^c}$, we obtain:

$$\delta W^3 = \left\langle \frac{1}{2}\sum_a \sum_c \sum_b \left. \frac{\partial k_{ij}^{\text{int},cb}}{\partial r_i^a} \right|_{r_i^a = \bar{r}_i^a} \delta r_i^a \left(r_j^b - \bar{r}_j^b\right)\left(r_k^c - \bar{r}_k^c\right) \right\rangle \tag{B.10}$$

Using the time independence of the derivative $\left. \frac{\partial k_{ij}^{\text{int},cb}}{\partial r_i^a} \right|_{r_i^a = \bar{r}_i^a}$, and further simplification, δW^3 may be rewritten as follows:

$$\delta W^3 = \frac{1}{2}\sum_a \sum_b \delta k_{ij}^{\text{int},ab} \beta_{ij}^{ab} \tag{B.11}$$

Now, the total work on the system may be obtained by summing δW^1, δW^2, and δW^3 to obtain:

$$\delta W = \sum_a -\bar{f}_i^{\text{int},a} \delta \bar{r}_i^a + \frac{1}{2}\sum_a \sum_b \left(k_{ij}^{\text{int},ab} - k_{ij}^{total,ab}\right)\left(\delta \beta_{ij}^{ab}\right) + \frac{1}{2}\sum_a \sum_b \delta k_{ij}^{\text{int},ab} \beta_{ij}^{ab} \tag{B.13}$$

Appendix C: Greens Function for Phonon Frequency Determination

The following derivation is for a periodic supercell of N atoms constructed with a primitive cell containing a single atom. Superscripts are used to indicate atom numbers and subscripts enumerate the Cartesian directions 1, 2 and 3. Under the harmonic approximation, the equation of motion for an atom in the supercell undergoing thermal vibration may be written as

$$m\ddot{u}_i = -\sum_b k_{ij}^{total,ab} u_j^b \tag{C.1}$$

where m is the mass of the aluminum atom, $\ddot{u}_i$ is the acceleration of atom a, $k_{ij}^{total,ab}$ are the components of the stiffness tensor for the interaction between atoms a and b, and u_j^b is the instantaneous displacement of atom b from its equilibrium position.

The particular solution to Eq. (C.1) is given by:

$$u_i^a = A_i e^{\left\{j\left[\vec{q}\cdot\vec{r}^a - \omega(\vec{q})t\right]\right\}} \tag{C.2}$$

where j is the unit imaginary number, A_i is the amplitude of the wave, $\vec{q}$ is the wavenumber, ω is the wave frequency, $\vec{r}^{\,a}$ is the position vector of the equilibrium position for atom a, and t is the time. Substituting Eq. (C.2) in Eq. (C.1), we get

$$\omega^2\left(\vec{q}\right)A_i = \sum_b k_{ij}^{total,ab} e^{\left\{-j\left[\vec{q}\cdot\left(\vec{r}^{\,a}-\vec{r}^{\,b}\right)\right]\right\}} A_j \tag{C.3}$$

Using the equivalence of all unit primitive cells (with one atom each), Eq. (C.3) may be rewritten as

$$\omega^2\left(\vec{q}\right)A_i = D_{ij}\left(\vec{q}\right)A_j \tag{C.4}$$

where $D_{ij}\left(\vec{q}\right) = \frac{1}{m}\sum_{ab} k_{ij}^{total,ab} e^{\left\{-j\left[\vec{q}\cdot\left(\vec{r}^{\,a}-\vec{r}^{\,b}\right)\right]\right\}}$ and the summation runs over all possible pairs for an atom including with itself.

The dynamical matrix is now determined using the approach proposed by Kong (83), and using the equipartition theorem (41) as follows

$$D_{ij}\left(\vec{q}\right) = \frac{1}{m}k_B T\left[\tilde{G}^{-1}\left(\vec{q}\right)\right]_{ij} \tag{C.5}$$

where $\tilde{G}\left(\vec{q}\right)$ is the Green's function in the reciprocal space given by

$$\tilde{G}_{ij}\left(\vec{q}\right) = \left\langle \tilde{u}_i\left(\vec{q}\right)\tilde{u}_j^{*}\left(\vec{q}\right)\right\rangle \tag{C.6}$$

The tilde signs refer to the Fourier transforms of the corresponding quantities and the * refers to the complex conjugate. The Fourier transforms of the atomic displacements can be written as

$$\tilde{u}_i\left(\vec{q}\right) = \frac{1}{\sqrt{N}}\sum_a u_i^a e^{-j\vec{q}\cdot\vec{r}_a} \tag{C.7}$$

$$\tilde{u}_j^{*}\left(\vec{q}\right) = \frac{1}{\sqrt{N}}\sum_b u_j^b e^{-j\vec{q}\cdot\vec{r}_b} \tag{C.8}$$

Noting that the equilibrium positions of atoms are independent of time, we substitute Eqs. (A.7) and (A.8) in Eq. (A.6), and simplify the Green's function to

$$\tilde{G}_{ij}(\vec{q}) = \frac{1}{N}\sum_{a}\sum_{b}\beta_{ij}^{ab} e^{-j\left(\vec{r}^{a}-\vec{r}^{b}\right)} \tag{C.9}$$

where $\beta_{ij}^{ab} = \left\langle u_i^a u_j^b \right\rangle$ is the second moment of atomic vibrations about their equilibrium positions.

Under conditions where every atom is identical in a periodic lattice, the Green's function in Eq. (C.9) is evaluated as $\tilde{G}_{ij}(\vec{q}) = \sum_{u}\beta_{ij}^{0u} e^{-i\vec{q}\cdot\left(\vec{r}^{0}-\vec{r}^{u}\right)}$, where $\beta_{ij}^{0u} = \frac{1}{N}\sum_{a=1}^{N}\beta_{ij}^{au}$ is the atomic average of the second moments, where 0 refers to the atom at the supercell origin.